Thermo-Mechanical Characterization of Motorola MMA1201P Accelerometer Test Report

Ashok. K. Sharma/NASA
Ashok.k.Sharma.1@gsfc.nasa.gov

Alaexander Teverovsky
QSS Group, Inc./NASA
Alexander.A.Teverovsky.1@gsfc.nasa.gov

Frederick Felt
QSS Group, Inc./NASA
Frederick.S.Felt.1@gsfc.nasa.gov

Part Description

Motorola MMA1201P is a single-axis, surface micromachined MEMS accelerometer rated for ±40 G and is packed in a plastic 16-lead DIP package. The operating temperature range is –40 °C to +85 °C with a storage temperature range of –40 °C to +105 °C. The part can sustain accelerations up to 2000 g from any axis while unpowered and powered accelerations up to 500 g.

The main components of the MMA1201P consist of a surface micromachined capacitive sensing cell (g-cell) and a CMOS signal conditioning ASIC. The g-cell's mechanical structure is composed of three consecutive semiconductor plates, defining sensitivity along the Z-axis (orthogonal to flat plane of the chip). When the accelerometer system is subjected to accelerations with components parallel to the sensitive axis of the g-cell, the center plate moves relative to the outer stationary plates, causing two shifts in capacitance, one for each outer plate, proportional to the magnitude of force applied. The shifts in capacitance are then processed by the CMOS ASIC, which determines the acceleration of the system (using switched capacitor techniques), conditions and filters the signal, and returns a ratiometric high voltage output.

A fourth semiconductor plate located in the g-cell allows testing of the accelerometer mechanics and electronics. When this plate is properly biased, an electrostatic force causes the movable plate to displace, causing changes in capacitance that can be processed by the CMOS ASIC as an acceleration, returning an output voltage proportional to the test plate bias. A fault latch, which is linked to the self-test system, can deactivate the accelerometer in cases of insufficient supply voltage, clock frequency, or changes in EPROM parity to odd. A rising edge on the self-test input pin will reset the latch.

Functional Block Diagram

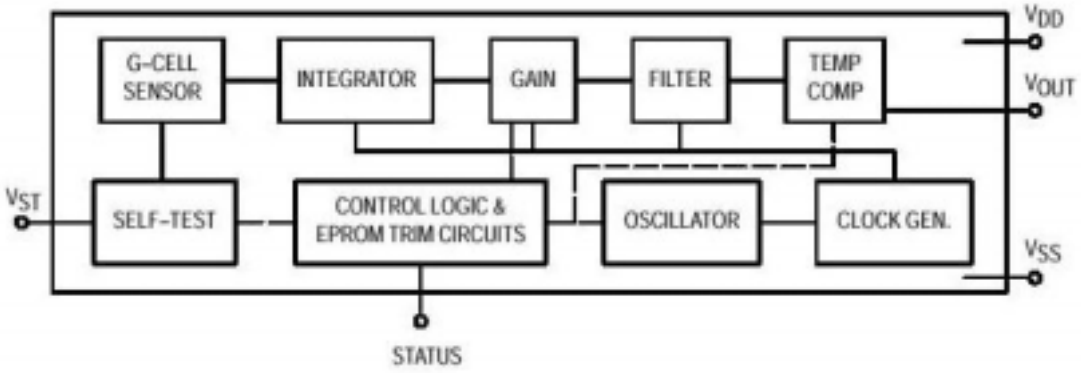

Pin Out Diagram

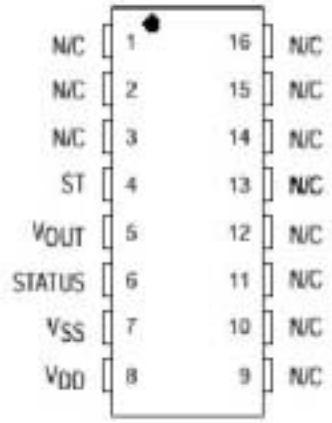

Pin No.	Pin Name	Description
1	—	Leave unconnected or connect to signal ground.
2 thru 3	—	No internal connection. Leave unconnected.
4	ST	Logic input pin to initiate self test.
5	V_{OUT}	Output voltage
6	Status	Logic output pin to indicate fault.
7	V_{SS}	Signal ground
8	V_{DD}	Supply voltage (5 V)
9 thru 13	Trim Pins	Used for factory trim. Leave unconnected.
14 thru 16	—	No internal connection. Leave unconnected.

Electrical Measurement Table

	Test Conditions	Min/Max Limits	Units
Output Voltage	VDD = 5V; T ≅ 21 °C; a = g_{Earth}	2.2 – 2.8	V
Supply Current	VDD = 5V; T ≅ 21 °C; a = g_{Earth}	4 – 6	mA
Sensitivity	a = g_{Earth} → 0 (rotate 90°)	47.5 – 52.5	mV/g
Status Output High	I_{LOAD} = 100 µA; Self-Test Logic High	> VDD - .8	V
Status Output Low	I_{LOAD} = -100 µA	< .4	V

Test Plan

I. Incoming Inspection
External examination, serialization, X-ray.

II. Thermal Cycling and Mechanical Shock
1. Low Range Thermal Cycle -40 to +105 °C (25 samples)
Electrical tests after 100, 200, 500, and 1000 cumulative cycles.

2. High Range Thermal Cycle -65 to +155 °C (25 samples)
Electrical tests after 30, 100, 200, 300, 500, 1000 cumulative cycles.

3. Mechanical Shocks 2000 g (20 samples)
Electrical tests after 30, 130, 430, 1430, 2500, 5000, 10000 cumulative shocks

III. Failure Analysis
All failed parts from cycling and shock tests were sent to FA for inspection.

Test Results

I. Thermal Cycling

Test results are shown in Table 1 and in Figure 1.

Table 1. Temperature cycling results showing proportion of failures (%) out of 25 samples tested.

Number of Cycles	Temperature interval	
	-40 +105°C	-65 +155°C
0	0	0
30	0	8
100	0	20
300	4	96
1000	4	

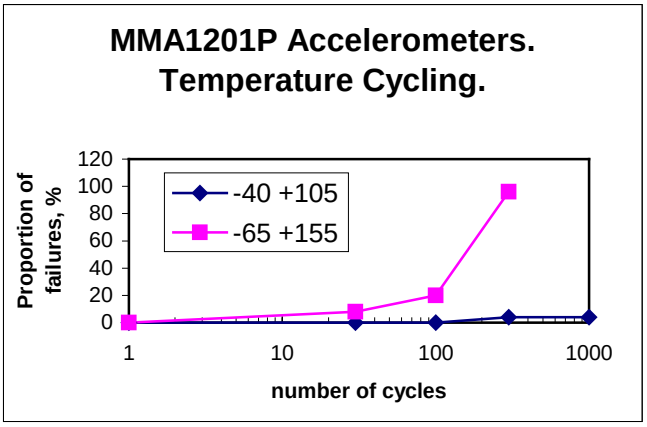

Figure 1. Temperature cycling test results showing proportion of Failures (%) versus number of cycles

II. Mechanical shock.

Test results are shown in Table 2.

Table 2. 2000 g Mechanical Shock Results. (25 samples).

Number of Shocks	Proportion of failures, %
0	0
30	0
130	16
430	20*
1430	20
2500	20
5000	20
10000	20

* one sample failed IDD high after 430 shocks, but then recovered after it was tapped several times, and showed normal IDD reading.

Summary and Conclusions

A total of 70 Motorola MEMS accelerometers were subjected to incoming inspection consisting of visual examination, serialization, X-Ray, Thermal Cycling within Low Range of -40 to +105°C (25 samples) and Thermal Cycling Extended Range of –65 to + 155°C (25 samples). Electrical test results were performed after 100, 200, 500, and 1000 cumulative cycles. Twenty parts were subjected to Mechanical Shocks (MS) of 2000 g with electrical tests after 30, 130, 430, 1430, 2500, 5000, 10000 cumulative shocks.

Test results showed no failures during low TC range testing till 100 cycles, and 4 % parts failing post 300 – 1000 TC electrical tests. During extended range TC testing, 8 % parts failed post 30 TC electricals and 96 % parts failed post 300 electricals. Mechanical shock testing showed no failures till 16 MS, and 16 – 20 % failures from 130 – 10,000 MS. These parts are not recommended for use in rugged environment and space flight applications.

The failed parts were subjected to failure analysis. Analysis indicated that temperature cycling caused the shrinkage of the internal silicon glop surrounding the sensor, resulting in broken internal wires and accelerometer failure. The failure mechanism for the parts failing shock testing has not been determined yet. However, the hybrid construction of the part suggests that multiple shocks in the z-axis might overstress the fragile silicon membrane of the transducer. Details are provided in the failure and construction analysis report in attached Appendix A.

Acknowledgements

This work was supported by NASA NEPP Program and was performed as a part of COTS MEMS Sensors/Accelerometers Quality and Reliability Characterization testing.

APPENDIX A

MOTOROLA MMA 1201P ACCELEROMETERS FAILURE AND CONSTRUCTION ANALYSIS REPORT

Motorola Accelerometers (MMA1201P) Failure and Construction Analysis Report

Background

An evaluation of plastic-encapsulated Motorola accelerometers was conducted for NEPP program. One group of parts were exposed to temperature-cycle testing, of 30 to 100 cycles. Another group of accelerometers was exposed to shock testing of between 200 and 430 shock events. Following these tests, electrical testing determined that many of the accelerometers had failed. The failing parts were forwarded to the GSFC Failure Analysis Laboratory for determination of cause of failure.

In addition, two untested parts were provided for construction analysis.

Part Description

The MMA1201P Motorola Accelerometer is a micomachined device featuring integral signal conditioning, linear output, and ratiometric performance. The part uses a 4^{th} order Bessel function filter to preserve pulse shape. It is calibrated for self-test. The transducer is hermetically sealed. The literature claims that the part is of a robust design, with high shock survivability. The parts are 16-pin DIPS in a plastic encapsulated package. No specifications for temperature extremes or shock are provided in the manufacturer's data sheets.

Analysis and Results

The parts were electrically tested to confirm the failures. It was observed that, of the parts subjected to temperature-cycling, all the failing parts failed due to the V_{off} parameter reading in the millivolt range, when the correct reading should have been approximately 2.5 volts. Similarly, the failing parts subjected to shock failed the V_{oH} parameter, read in the millivolt range, where as the correct reading should have been approximately 5.0 volts. Therefore, the pattern of electrical failures suggested a common failure mode for temperature-cycling, and a second common, but different, failure mode for shock test.

The parts were examined externally and photo-documented. No anomalies were found. The parts were x-rayed, revealing that the accelerometer essentially had a hybrid construction, and consisted of a microcircuit and an internal sensor/transducer. Gold bond wires connected the microcircuit to the external lead frame, while internal wires linked the microcircuit to the sensor.

Careful examination of the x-ray images under magnification revealed that some of the internal wires on the parts receiving temperature-cycle testing appeared to be broken near the edge of an internal cavity. These wires were also kinked on one end, near an internal bonding pad on the sensor. The portion of the wires remaining inside the plastic encapsulation had a nominal, undamaged appearance.

In comparison, x-rays did not reveal any damage to the wires of the parts subjected to shock testing. Nor was there any evidence of wire damage in the x-rays of the untested parts submitted for construction analysis.

Mechanical lapping was used to remove the top surface of the plastic encapsulation and reveal the wires underneath. It was found that the internal cavity was filled with a clear polymer, possibly a silicone material, through which the wires could be partially inspected once the plastic encapsulation had been removed. The parts were inspected optically in both top-down and side views. In the group of parts subjected to temperature-cycle testing, it was determined that many wires were severely kinked at the bonding pads. Closer inspection suggested that the breakage had also occurred at the bond heel. In addition, some of the wires were confirmed to be broken or damaged near the silicone/plastic interface, where evidence of neck-down was also found, as if the damaging process had been interrupted prior to breakage.

The nature of the damage suggested that the silicone had shrunk and expanded under multiple temperature cycles and, while doing so, the silicone had pulled anisotropically on the gold wires, leaving them damaged after testing. Multiple temperature cycles caused the wires to kink and break at the bond pads, and caused Poisson necking at the silicone/plastic interface. A gap was also seen between the silicon and the plastic, indicating lack of adhesion between the plastic and the silicone.

In comparison, no evidence of damage to the wires was found during optical inspection of the accelerometers subjected to shock testing.

Various methods of chemical removal of the silicone were tested and found ineffective.

Several of the parts were cross-sectioned. A thin cavity was discovered between the two sandwich plates of the sensor. The cavity was back-filled. Subsequent cross sectioning and SEM views revealed internal features of microcircuitry, but these features were difficult to identify in a cross sectional view. The material holding the two layers of the sensor together was identified by EDS, as predominately lead.

A sensor was extracted from its encapsulating silicone and photo-documented. Its construction suggested that the sensor had been glued to the lead frame, then encapsulated under a silicone drop, and then the whole part, including lead frame and microcircuit, was subjected to plastic encapsulation.

One of the sensors was selected for destructive deprocessing. After removal of the glue and silicone, the sensor was attached to a metal wand and carefully split open using a microscope and a razor.

Internal SEM and EDS inspection revealed that the accelerometer sensor consists of a silicon membrane supported at four corners. This membrane stands above another silicon layer on the substrate. The sensor apparently works because of capacitance changes as the membrane deflects under acceleration. The lid of the cavity appears to form one plate of the capacitor. Also the substrate may form another plate. Four serpentine resistors and pads were observed on the substrate near the center of the transducer. A long integration EDS of the membrane indicated virtually pure silicon with a trace of cobalt.

While the cause of failure for the shock-tested parts has not yet been determined, it is suspected that shock in the z-axis direction may have caused damage to the unsupported silicon membrane.

Failure Analysis Conclusions

Temperature-cycle testing caused the shrinkage of the internal silicone glop surrounding the sensor, resulting in broken internal wires and accelerometer failure

The cause of failure of the parts damaged during shock-testing has not yet been determined. However, the construction of the part suggests that multiple shocks in the z-axis might have overstress the fragile silicon membrane of the transducer.

Figure 1. An external top view of the accelerometer manufactured by Motorola. 5X

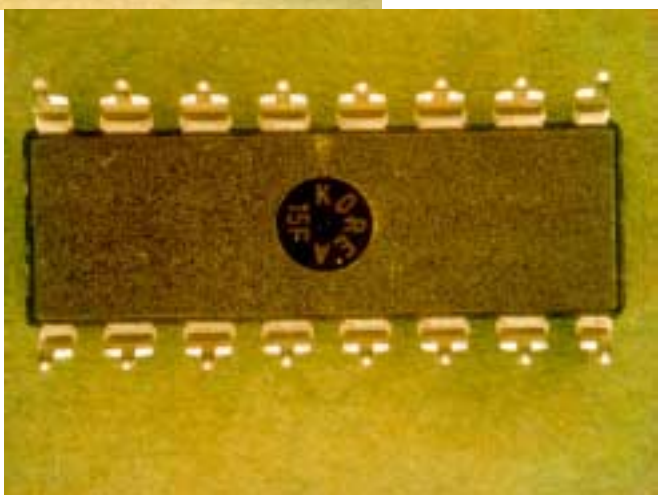

Figure 2. An external bottom view of the accelerometer. 5X

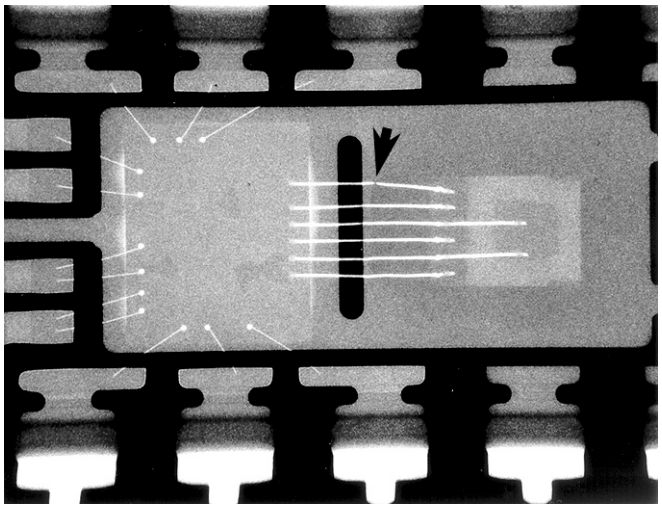

Figure 3. X-ray view of accelerometer reveals that it is a hybrid device. A large microcircuit at left is wire-bonded to the lead-frame. Internal wires bridge to the sensor. Arrow indicates defect seen better in Figure 4. 10X

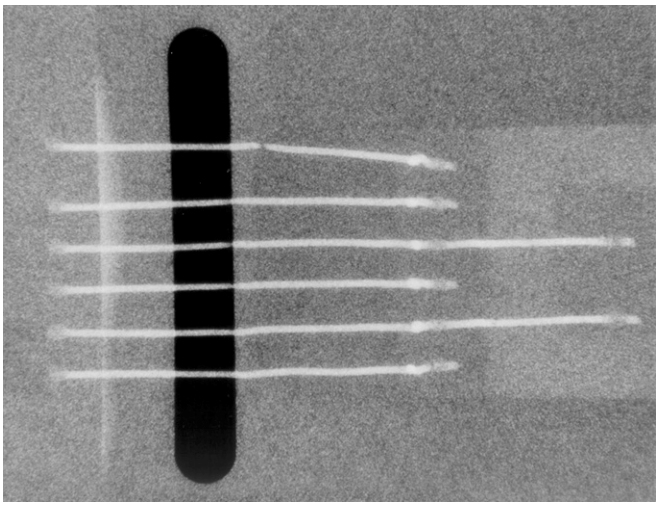

Figure 4. Close examination of the bridging wires inside the part reveals an apparent break in the top wire in this photo. The large, faint shadow over the sensor indicates the cavity filled with silicone. Note that wire break occurs near the interface of the plastic and the silicone. SN76 failed under temperature-cycle testing. 25X

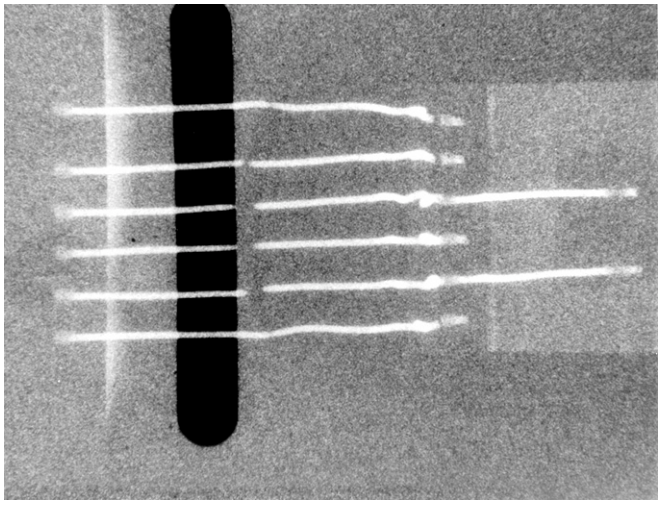

Figure 5. A similar, but more severe problem was noted on SN78, which also underwent temperature-cycle testing. Many of the above wires are broken. All of the wires appear wavy or kinked on the right. 25X

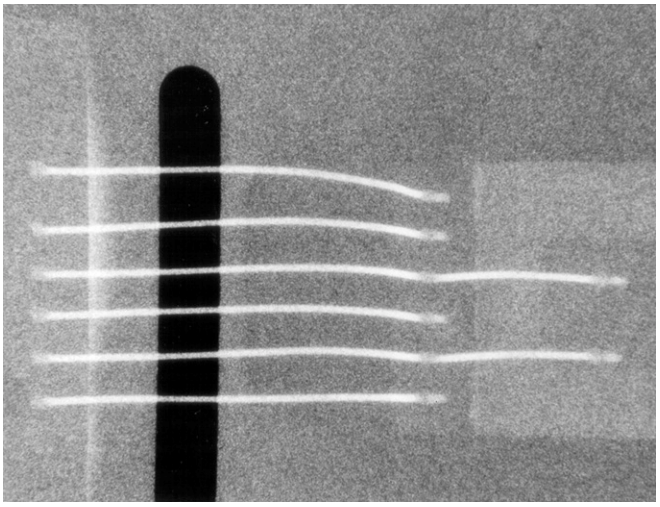

Figure 6. A second group of accelerometers failed due to shock. This representative device x-ray shows no evidence of wire breakage or kinking. 25X

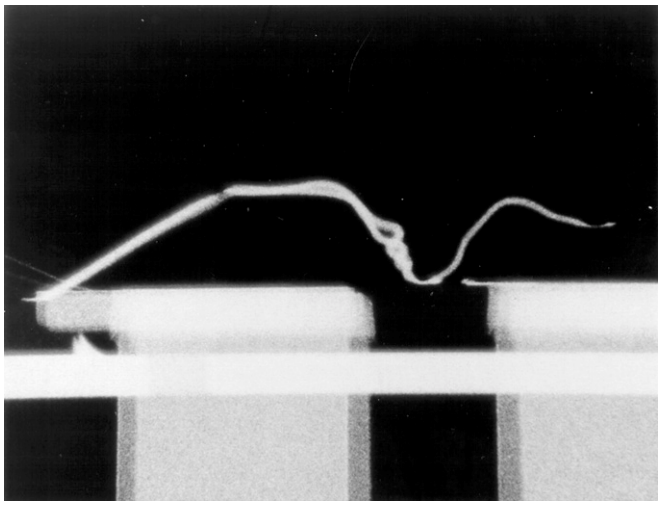

Figure 7. The bridging wires are seen in side view in this x-ray of SN78. Most of the wires broke at a common location near the edge of the cavity. Note that on the left of the break the wire is smooth; on the right it is kinked. 25X

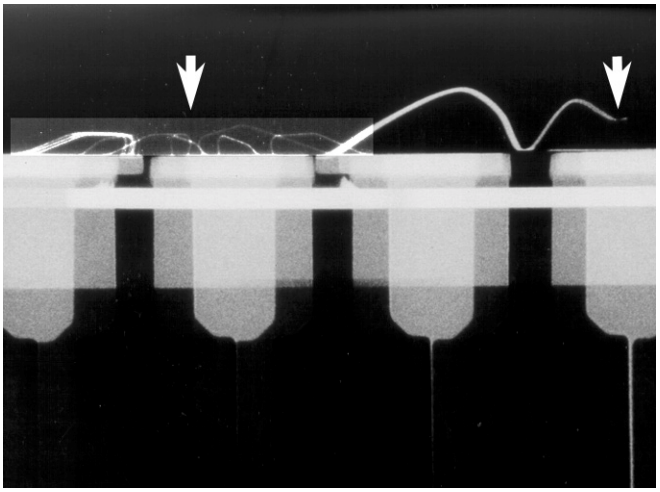

Figure 8. SN264 failed due to shock. Notice that the wires are not damaged. The arrow on the left points to an enhanced region showing the lead dress of the wires bonded between the lead frame and the microcircuit. Arrow on the right indicates where the wires attach to the top of the sensor, which cannot be seen in this x-ray. 25X

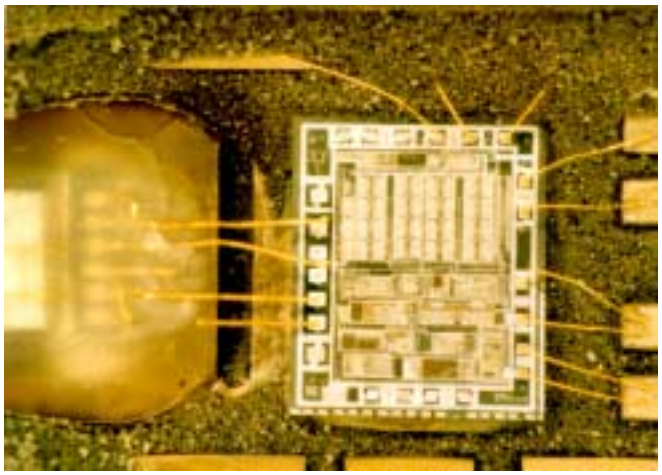

Figure 9. Internal view of the accelerometer with the plastic encapsulation chemically removed, causing some bending of the wires. The sensor is seen on the left in this view, under a glop of silicone made translucent by chemical action. 13X

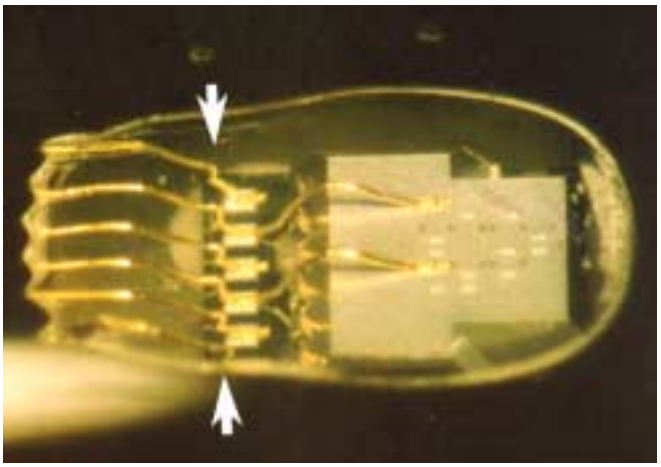

Figure 10. The SN76 sensor is seen on the right, under two wire bonds. The plastic encapsulant was lapped off in this method of deprocessing, revealing clear silicone underneath. Note that gold wires between arrows are kinked.

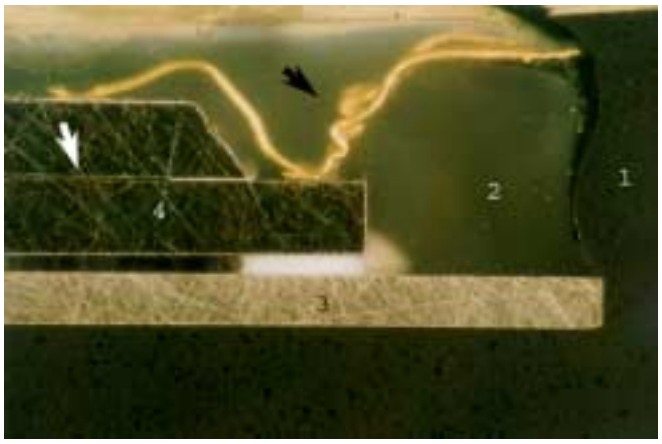

Figure 11. This side view of sensor and wires reveals construction of SN76. (1) Plastic encapsulant. (2) Silicone inside cavity. (3) Lead frame. (4) Sensor. Note that sensor has a two-part construction, with a space in between as indicated by the white arrow. Black arrow points at kinked wires. 32X

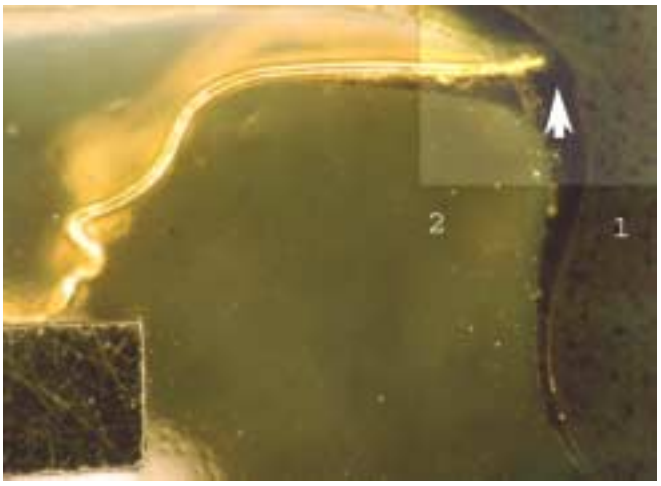

Figure 12. Close-up view of wires in Figure 11, showing severe kinking. Note that a space exists between the plastic (1) and the silicone (2). Enhan-ced corner of photograph highlights the gap and shows that the wire is slightly tapered at its end, and broken, as the wire does not extend to the plastic. 64X

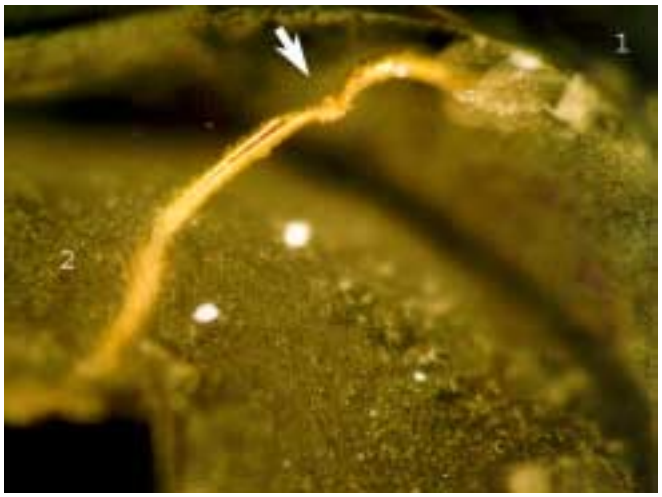

Figure 13. The gap between the plastic (1) and silicone (2) is seen in this view of SN77. Arrow points to a wire region inside the gap which exhibits necking. 64X

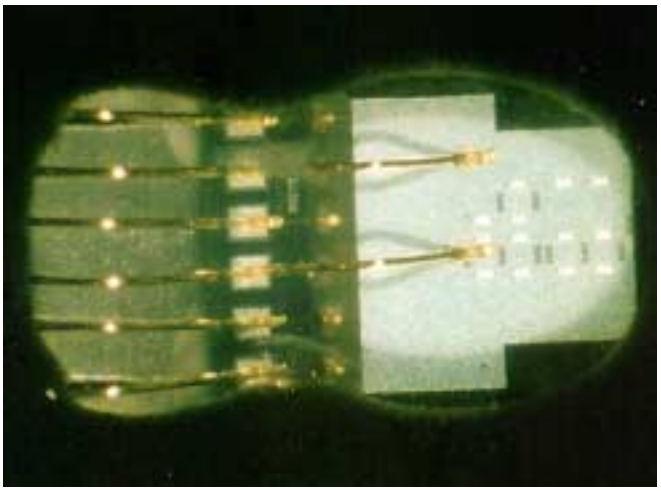

Figure 14. Another view of a part which did not experience temperature-cycling. SN262 failed shock testing. Observe that the wires are continuous and smooth, with no evidence of breakage or kinking. 16X

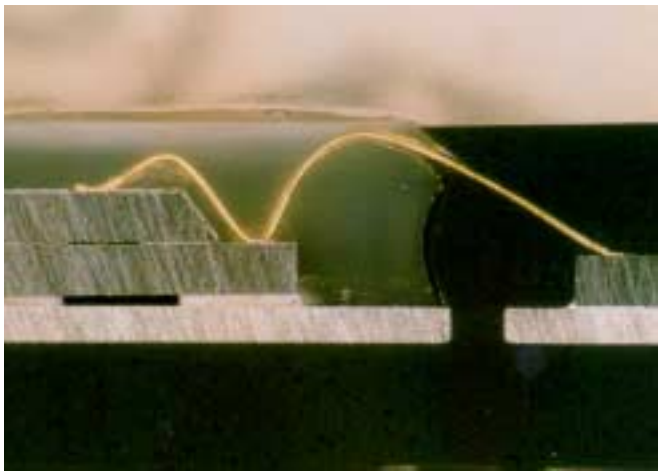

Figure 15. A side view of SN262 indicates the wires are in excellent condition, unlike the parts that experienced temperature-cycle testing. 16X

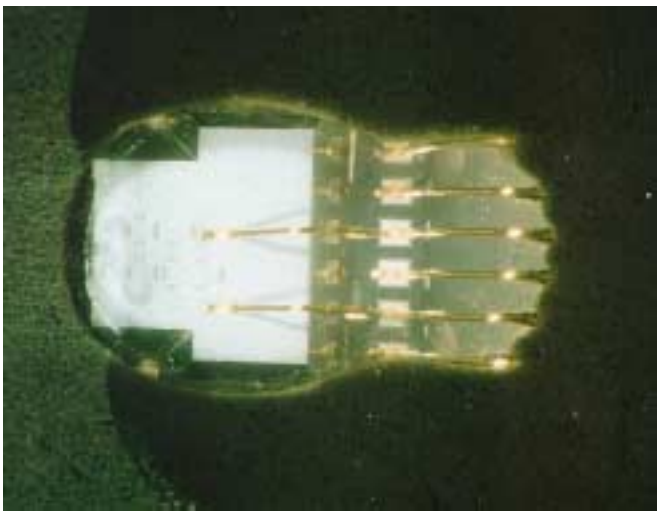

Figure 16. SN281 was submitted for construction analysis. Note that the wires of the device, as manufactured, appear unbroken and smooth. 16X

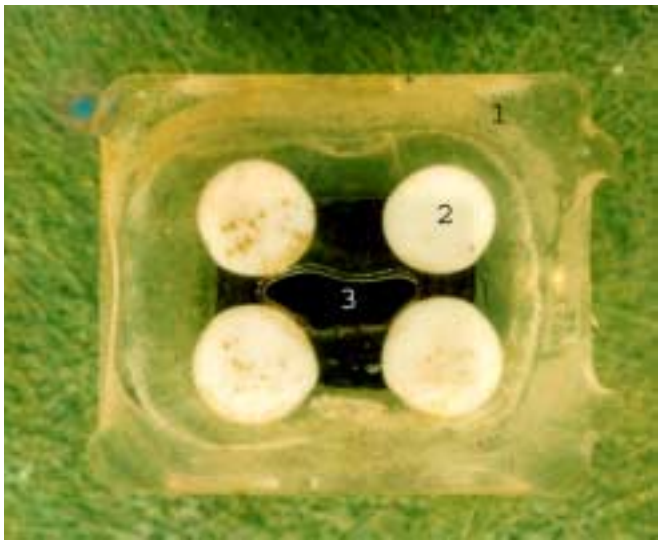

Figure 17. Inverted view of sensor (3), showing the silicone (1), and four white, apparently polymer glue feet (2). 16X

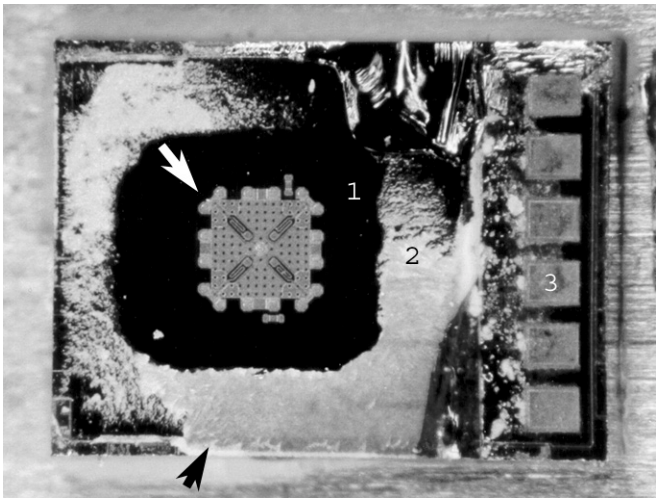

Figure 18. Black arrow indicates silicon substrate in this view of the sensor after destructive opening. White arrow indicates the actual accelerometer. (1) Cavity. (2) Lead bonding material. (3) Bond pads. 32X

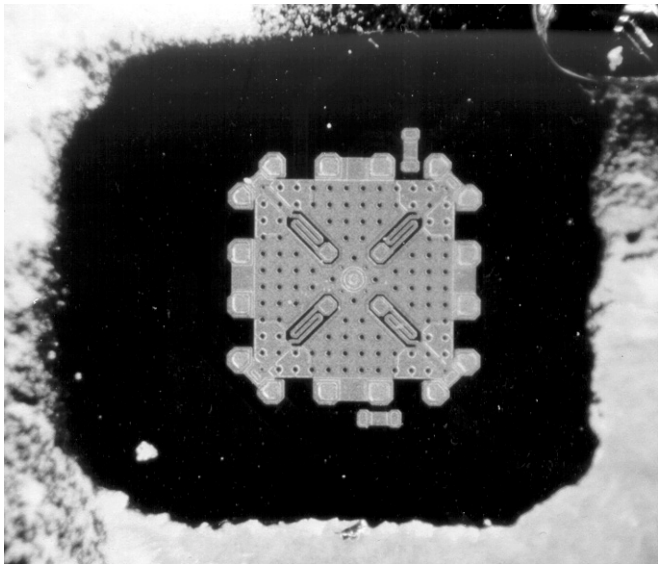

Figure 19. Optical view of accelerometer sensor inside cavity. 64X

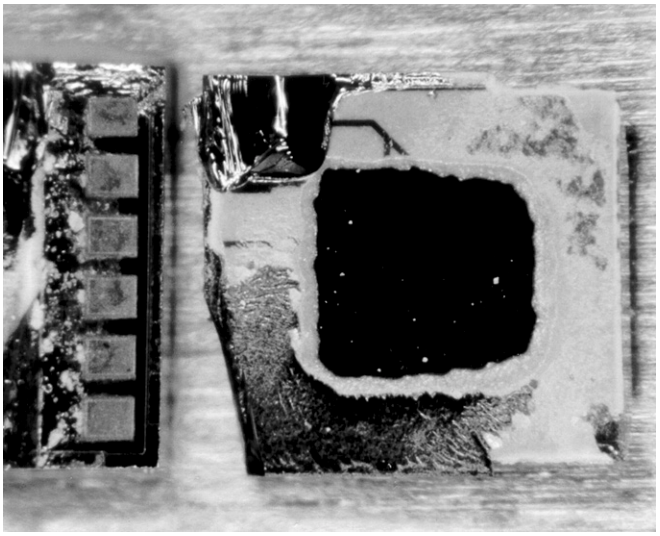

Figure 20. The lid of the sensor is shown on right. Note that an electrical trace appears to connect with the dark surface, which is presumably conductive. 32X

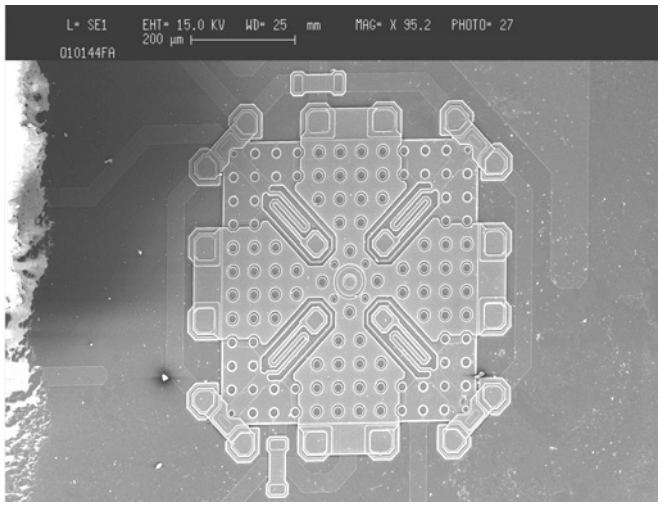

Figure 21. SEM view of sensor inside cavity. 95X

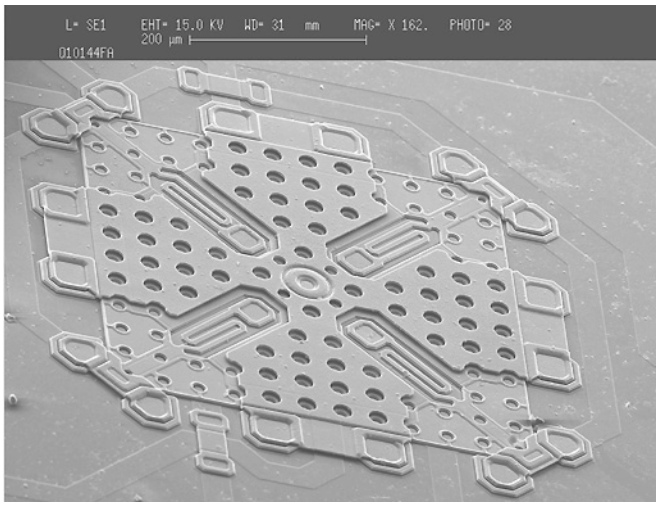

Figure 22. Tilt SEM view of sensor. Note the two bridges on opposite sides of the sensor, and the faint, apparently diffused traces. 162X

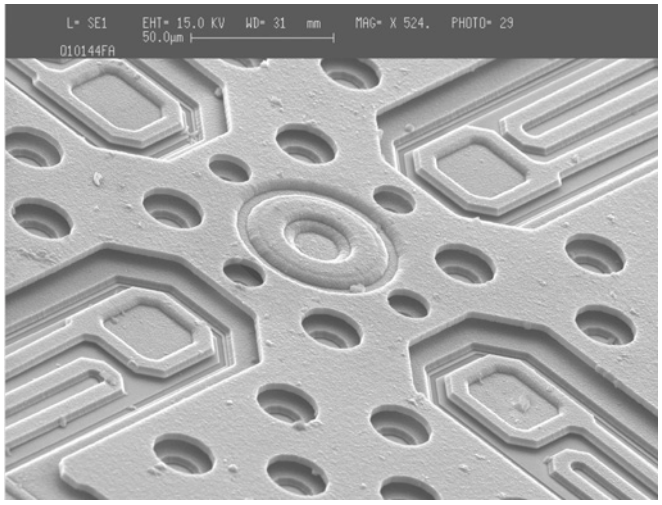

Figure 23. The center of the sensor appears to be a suspended membrane. Four pads on the lower level are also seen. 524X

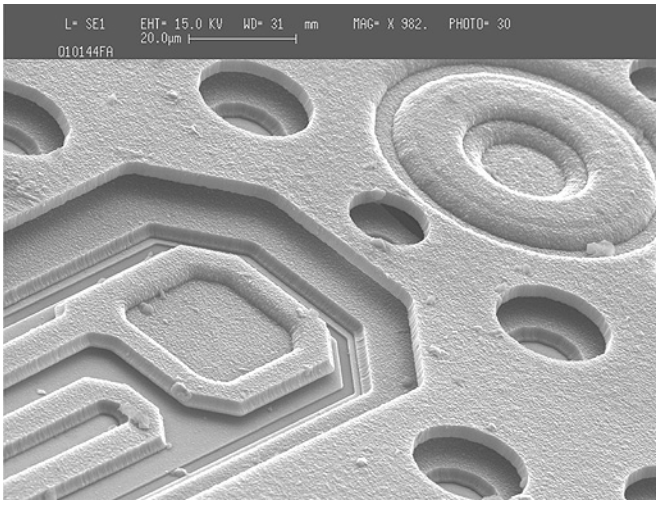

Figure 24. The membrane is clearly elevated in this view. Round holes on both the upper and lower levels, may be intended for the etching process, and also to make the membrane more flexible. EDS showed that the membrane was silicon with a trace of cobalt. 982X

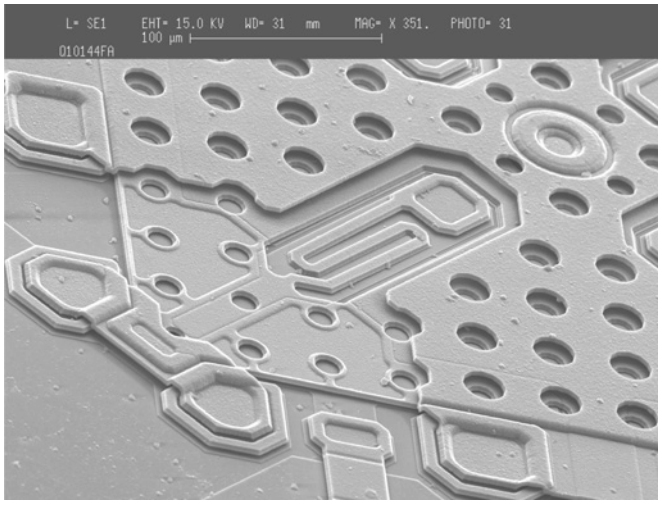

Figure 25. A corner view of the sensor. EDS indicated that the lower level was also composed of silicon. Serpentine path appears to be a resistor connecting to a pad. 351X

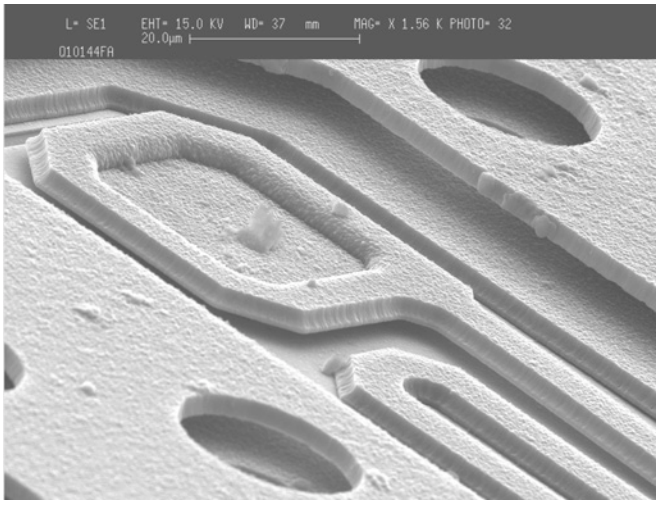

Figure 26. Close-up of the pad. The membrane appears suspended in this high-angle view. 1560X

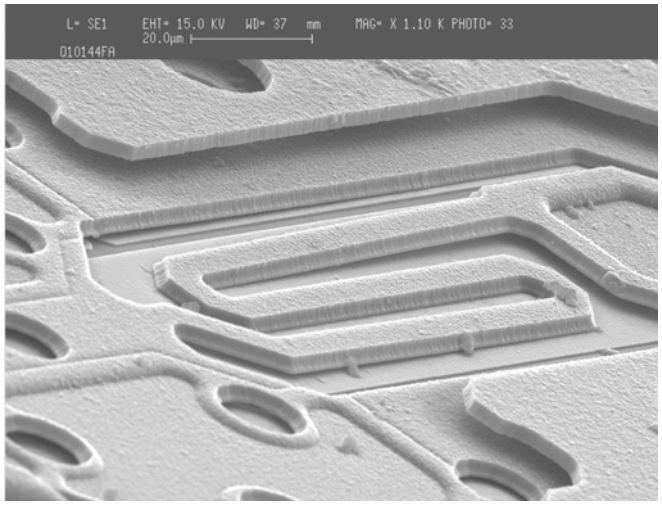

Figure 27. Note that the lower level of silicon appears to be elevated at the left end, behind the resistor, while also being down at the right side, creating a gentle slope. It is not understood if this is an artifact of the manufacturer's etching process, or necessary for the device operation. 1100X

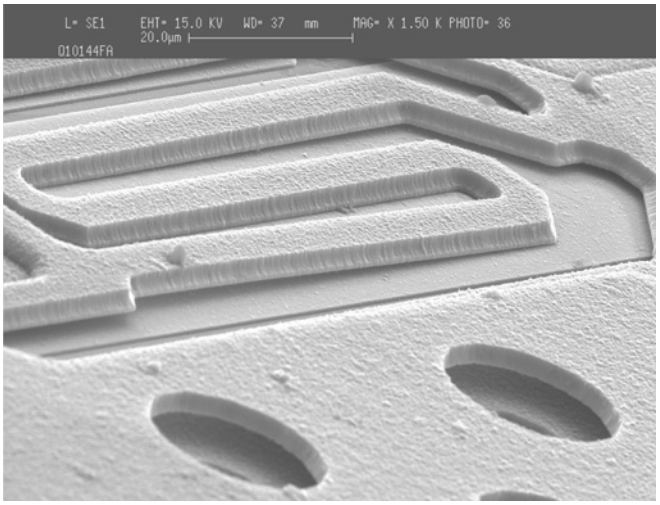

Figure 28. Close-up of resistor. An edge of the membrane is in the foreground. Note the slope on the resistor, while the pad, itself is intimate with the substrate. 1500X

Figure 29. The trace at the upper left appears to go nowhere. 510 X

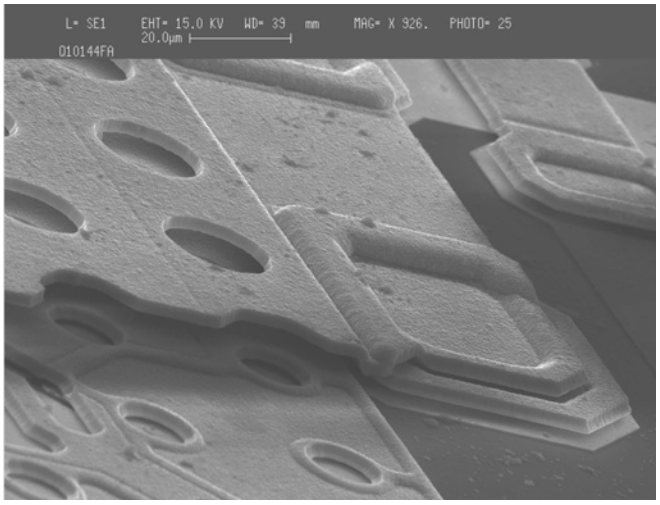

Figure 30. A high angle view of a corner where membrane appears to be suspended. It is suspected that shock in the z-axis may have damaged the membrane of the parts exposed to shock testing. 926X

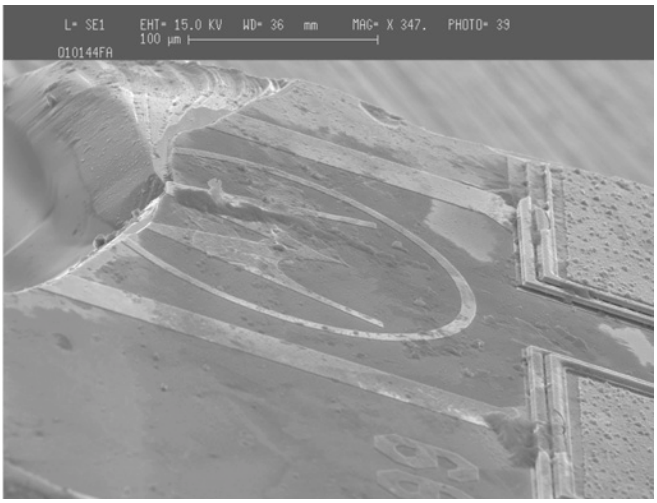

Figure 31. Motorola logo. 347X